Integrated Local Correlation: A New Measure of Local Coherence in fMRI Data

Gopikrishna Deshpande, Stephen LaConte, Scott Peltier, and Xiaoping Hu*

WHC Department of Biomedical Engineering, Georgia Institute of Technology and Emory University, Atlanta, Georgia

◆ ══════════════════════════════════ ◆

Abstract: This article introduces the measure of integrated local correlation (ILC) for assessing local coherence in the brain using functional magnetic resonance imaging (fMRI) data and characterizes the measure in terms of reproducibility, the effect of physiological noise, and the dependence on image resolution. The coupling of local neuronal processes influences coherence in a voxel's neighborhood. ILC is defined, for each voxel, as the integration of its spatial correlation function. This integrated measure does not require the specification of a neighborhood and, as demonstrated by experimental data, is effectively independent of image resolution. Respiratory and cardiac fluctuations do not considerably alter the ILC value except in isolated areas in and surrounding large vessels. With resting-state fMRI data, ILC was demonstrated to be tissue-specific, higher in gray matter than white matter, and reproducible across consecutive runs in healthy individuals. Within the gray matter, ILC was found to be higher in the default mode network, particularly the posterior and anterior cingulate cortices. Comparing ILC maps obtained from resting state and continuous motor task data, we observed reduced local coherence in the default mode network during the task. Finally, we compared ILC and regional homogeneity by examining their ability to discriminate between gray and white matters in resting state data and found ILC to be more sensitive. *Hum Brain Mapp 30:13–23, 2009.*   © 2007 Wiley-Liss, Inc.

Key words: functional MRI; local coherence; spatial correlation; resting-state fMRI; tissue-specificity

◆ ══════════════════════════════════ ◆

INTRODUCTION

Functional connectivity [Friston et al., 1993] between anatomically distributed regions of the brain in resting-state has been well studied using neuroimaging techniques including functional magnetic resonance imaging (fMRI). Most functional connectivity studies focus on connectivity between different regions in networks. On the other hand, local coherence carries information regarding localized coordination among neighboring neuronal units and is dependent on the local anatomic structure and homogeneity of neuronal processes. This aspect has been investigated recently by a regional homogeneity (ReHo) measure [Zang et al., 2004] derived using Kendall's coefficient of concordance (KCC) [Baumgartner et al., 1999; Kendall and Gibbons, 1990]. In their study, Zang et al. found significant changes in ReHo in a finger tapping experiment. In a more recent study, Kriegeskorte et al. [2006] showed that improved functional activation maps could be obtained using an information-based approach incorporating the local functional homogeneity but avoiding spatial smoothing.

Methodologically, previous studies of local coherence utilized predefined neighborhoods, making the result explicitly dependent on the neighborhood size and implicitly on the spatial resolution. In this work, we introduce a general approach to characterize local brain coherence by defining a

metric, integrated local correlation (ILC), which is the integration of the spatial correlation function for each voxel. In principle, the integration does not require the specification of a finite neighborhood. In practice, the spatial correlation function becomes negligible beyond 25–43 mm limit of "local scale" defined by Bellec et al. [2006] except in cases of distributed networks, which are not the focus of this study. Therefore, for the practical implementation of ILC calculation, only a finite neighborhood needs to be considered. Although the spatial correlation function for a voxel is a continuous function in principle, it can only be measured discretely in practice at the acquired image resolution. This is a potential problem for ReHo [Zang et al., 2004] because KCC is dependent on ranking, which is sensitive to the number of voxels in the neighborhood, and hence indirectly dependent on resolution. This problem is negligible for ILC, because the integration of the entire correlation function with respect to the physical dimensions is not expected to depend on the sampling resolution significantly.

Resting-state fluctuations in fMRI have gained significant interest because they are thought to carry vital physiological information. In fact, low frequency correlation between distributed regions is being extensively used in examining functional connectivity in networks [Biswal et al., 1995, 1997; Cordes et al., 2000; Hampson et al., 2002; Lowe et al., 1998; Peltier and Noll, 2000]. Therefore, local coherence in resting state may provide an added measure for understanding the brain. To demonstrate that ILC is a meaningful measure, we examined its tissue specificity and reproducibility in resting state fMRI data. To demonstrate that ILC does not arise primarily from fluctuations due to heart beat and respiration, we also compared ILC derived with and without the removal of physiological noise. Our results show that ILC is tissue-specific, reproducible, has functional relevance, and not greatly influenced by physiological fluctuations. Comparing ILC maps obtained from resting state and a continuous motor task revealed reduced local coherence in the default mode network during the task thereby demonstrating the utility of ILC for differentiating experimental conditions. Finally, we compared ILC and ReHo by examining their ability to discriminate between gray and white matter in resting state data and found ILC to be more sensitive.

METHODS

Definition and Calculation of ILC

With local coherence attributed to physical proximity, the temporal correlation of a given voxel with its neighbors is a function that decreases with distance and can be used to characterize the local coherence. In this work, the spatial correlation function is integrated, giving rise to ILC, to characterize local coherence. In the two-dimensional (2D) case considered here, ILC reflects the volume under the spatial correlation function. Note that the integration of the correlation function, which goes to zero rapidly with distance, is insensitive to the size of the neighborhood used for the integration as long as it is sufficiently large. This would not be the case if the mean of the correlation function in the neighborhood is used.

Given that our measurement of the correlation function is discrete and truncated, it is desirable for any measure of local coherence to be independent of discretization and truncation. Although the definition of ILC suggests this independence, it needs to be experimentally verified. Discretization is dictated by the finite spatial resolution of image acquisition. If the correlation function is sufficiently smooth, the ILC obtained should be independent of the spatial resolution. This hypothesis is tested experimentally with data obtained at two spatial resolutions.

Even though we have considered the 2D case in this report, ILC could theoretically be extended to the three-dimensional (3D) case if we have contiguous slices. These voxels would not need to be isotropic based on our demonstration of insensitivity to voxel size. However, with multi-slice imaging, issues of imperfect slice profile and slice timing would have to be considered and may make the ILC calculated in 3D more complicated.

Data Acquisition

In the first experiment, echo planar imaging (EPI) data were obtained from a phantom containing a solution of 3.75 g $NiSO_4$ and 5 g NaCl in 1,000 g H_2O, using a 3.0 T Siemens Trio scanner. The scan parameters were repetition time (T_R) = 750 ms, echo time (T_E) = 34 ms, flip angle (FA) = 50°, field of view (FOV) = 22 cm, five slices with a thickness of 5 mm, 280 volumes per slice, and an in-plane resolution of 3.44×3.44 mm^2.

In Experiment 2, resting state EPI runs were obtained in three healthy subjects while they were instructed to keep their eyes open, fixate on a central cross, and not engage in any mental activity. Three consecutive scans were performed with parameters similar to those used in the phantom experiment: T_R = 750 ms, T_E = 34 ms, FA = 50°, FOV = 22 cm, 10 axial slices of 5 mm thickness covering the section between the corpus collusum and the top of the brain, 280 volumes per slice, and an in-plane resolution of 3.44×3.44 mm^2. In addition, a high-resolution resting-state scan was also performed with an in-plane resolution of 2×2 mm^2 and other EPI parameters matched to the first three scans. T_1-weighted anatomical images with 1 mm isotropic resolution were acquired using a magnetization prepared rapid gradient echo (MPRAGE) sequence [Mugler and Brookeman, 1990] with T_R/T_E = 2600/3.93 ms and FA = 8°.

In the third experiment, resting-state data were acquired in three subjects using the scan parameters described earlier, with the difference that only five slices were acquired. These slices started at the top of the brain with a voxel size of $3.44 \times 3.44 \times 5$ mm^3. A pulse-oximeter and nasal respiratory cannula were used during data acquisition to obtain cardiac and respiratory pulsations, respectively. T_1-weighted axial anatomical images were acquired in the same slices at an
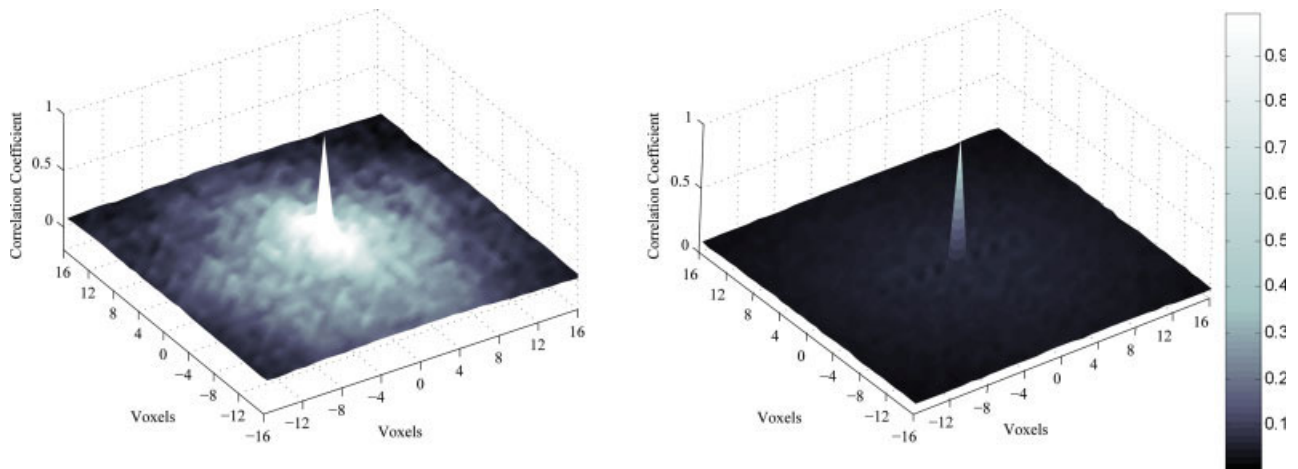
Figure 1.

Mean spatial correlation functions. Left: brain tissue. Right: EPI phantom. [Color figure can be viewed in the online issue, which is available at www.interscience.wiley.com.]

image resolution of 512×512 using a spin-echo sequence ($T_R = 534$ ms, $T_E = 8.6$ ms, and FA = 90°).

In the fourth experiment, EPI data were acquired in three healthy volunteers with a paradigm consisting of 3 min of a fixation condition (resting state) followed by 3 min of a continuous motor task that required the subjects to continuously perform bimanual finger opposition. The finger opposition was paced at 1 Hz by a number (1, 2, 3, or 4) visually presented, indicating the digit to oppose against the thumb. Scan parameters were $T_R = 750$ ms, $T_E = 34$ ms, FA = 50°, and FOV = 22 cm. The volume imaged consisted of 10 axial slices of 5 mm thickness covering the section between the bottom of the corpus collusum and the top of the brain. The resting and task periods each consisted of 280 time points. In addition, T_1-weighted anatomical images with 1 mm isotropic resolution were acquired using an MPRAGE sequence [Mugler and Brookeman, 1990] with $T_R/T_E = 2600/3.93$ ms and FA = 8°.

Data Analysis

The operational procedure for calculating ILC is as follows. Motion correction and slice scan time correction was performed. Subsequently, detrending was applied to each voxel time series to remove baseline drift. For each voxel in the image, a 2D correlation function corresponding to its temporal correlation with neighboring voxels was calculated (Fig. 1) and integrated to obtain ILC as given in the equation below.

$$\text{ILC}(\vec{s}) \cong \sum_x \sum_y \frac{\sum_{n=0}^{N-1} \left[a_{\vec{s}}(n) \times b_{xy}(n) \right]}{\sqrt{\sum_{n=0}^{N-1} \left[a_{\vec{s}}(n) \right]^2 \times \sum_{n=0}^{N-1} \left[b_{xy}(n) \right]^2}}$$

where $\vec{s}$ is the position of the voxel under consideration, and $a_{\vec{s}}(n)$ is the time course for that voxel. $b_{xy}(n)$ represents all other neighboring voxels where x and y span the

dimensions of the neighborhood. ILC was calculated only for those voxels for which the neighborhood used for the calculation was contained within the image. In addition, as described below, a correction to account for system inherent correlation was determined and applied to the resultant ILC. The ILC was calculated for every voxel in the image to form ILC maps. The anatomical images were manually segmented into gray matter and white matter using MRIcro [Rorden and Brett, 2000], a freely available medical image processing software package (http://www.sph.sc.edu/comd/rorden/mricro.html). The segmented images were down-sampled to match the EPI resolution and separate gray matter and white matter masks were obtained and used in assessing the tissue-specificity of ILC.

Characterization of ILC

Inherent correlation in fMRI data and its correction

It is possible that fMRI data contain inherent correlation due to the image acquisition and reconstruction processes. To ascertain the possible inherent correlation in the data and its effect on ILC, the spatial correlation function of the phantom data and the corresponding ILC maps were obtained and examined. Furthermore, the distribution of the phantom ILC was compared with that of a simulated independent Gaussian random field with matching standard deviation using the Wilcoxon rank sum test. It was found that the inherent correlation was small but could not be ignored. To compensate for this effect, the spatial correlation function of the phantom, obtained by averaging the correlation function of all voxels in the phantom, was subtracted from the spatial correlation function of each pixel in the human brain data before ILC calculation.
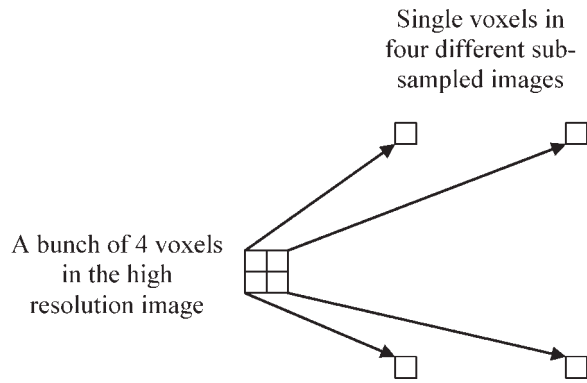
Single voxels in
four different sub-
sampled images

A bunch of 4 voxels
in the high
resolution image

Figure 2.

A schematic illustrating the sub-sampling scheme used to derive low-resolution images from high-resolution data.

Discretization and truncation

To investigate the effect of resolution on the calculated ILC, we used the high-resolution EPI data with the matrix size of 128×128. The in-plane resolution for this data set was 2×2 mm^2. To obtain ILC maps calculated with low-resolution images, the k-space data of the high-resolution images were truncated to a 64×64 matrix, zero padded to 128×128, and inverse Fourier transformed to form an image that had a resolution of 4×4 mm^2 but a matrix size of 128×128. This image was divided into four nonoverlapping 64×64 sub-images using the simple sub-sampling scheme shown in Figure 2. Each of these sub-sampled images was used to calculate an ILC map, using a neighborhood that has the same physical size as that used for the high-resolution image. The resultant maps
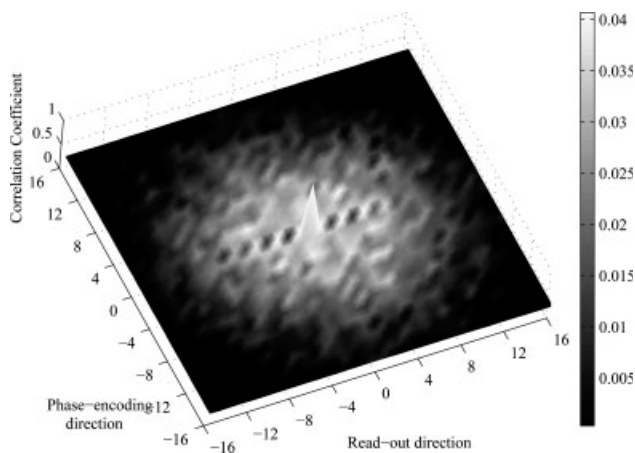
were combined by reversing the down sampling process, providing a 128×128 ILC map for comparison of mean ILCs in gray matter and white matter Region of Interest (ROIs). Note that this process allowed us to calculate the ILC map with low-resolution images and to perform the comparison at the same high resolution. To examine the effect of truncation, the earlier process was repeated for neighborhood sizes ranging from 12×12 mm^2 to 68×68 mm^2 (corresponding to 3×3 to 17×17 low-resolution voxel neighborhoods).

Effect of physiological noise

The effect of cardiac and respiratory pulsations on fMRI data has been extensively studied [Deshpande et al., 2006; Hu et al., 1995; Kruger and Glover, 2001]. To test the effect of physiological fluctuations, data from Experiment 3 were analyzed with and without physiological noise correction using a retrospective technique [Hu et al., 1995]. ILC maps were obtained before and after the correction and the significance of the difference was ascertained.

Tissue-specificity

Gray matter and white matter masks were obtained as described in the Data Analysis section and were used to obtain mean ILC values for the gray matter and white matter, respectively. In addition, the ILC maps were upsampled to the resolution of the anatomical image and overlaid on it.

Regional ILC differences in gray matter

Using EPI data obtained from the three subjects in the second experiment, the mean ILC value of gray matter for each of the three runs was calculated. The statistical significance of the difference between the ILC value of each voxel and the gray matter mean ILC was ascertained and displayed as a statistical parametric map. For every sub-
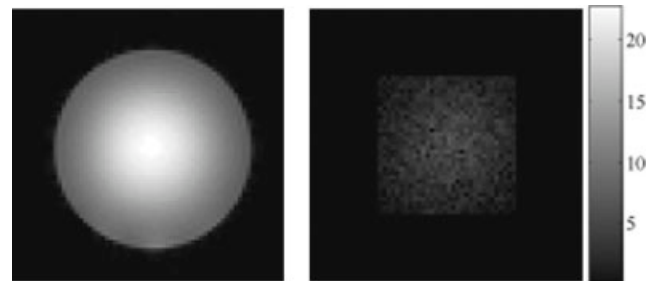
Figure 3.

Rescaled spatial correlation function of the phantom showing *sinc*-modulation in the readout direction. The original scale (0, 1) is compressed to (0, 0.04) in this figure.

Figure 4.

Left: EPI phantom image obtained with parameters matched to in vivo data. Right: ILC image of EPI phantom plotted on a matched scale. The images are representative of a typical slice and other slices also gave similar results.
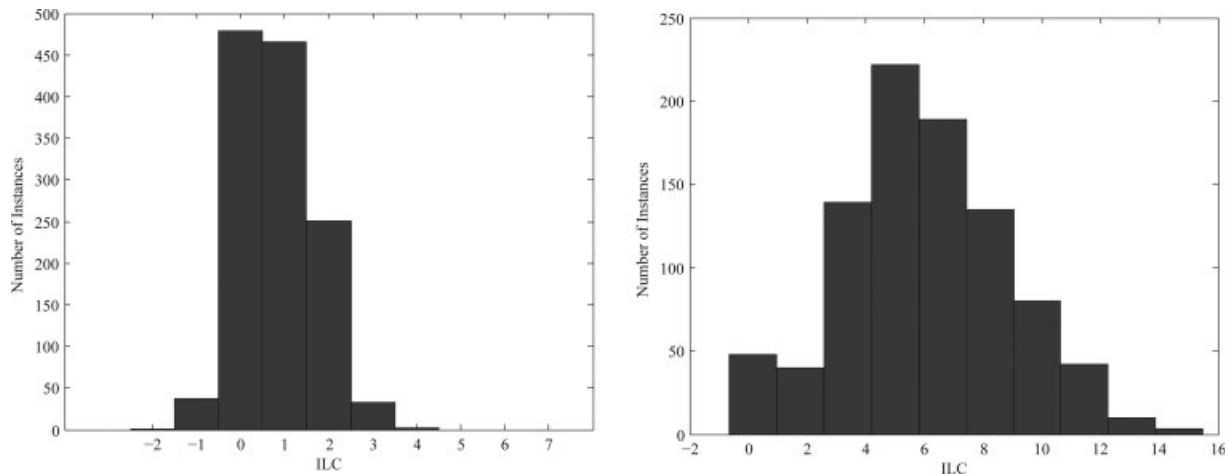
Figure 5.

Left: ILC null distribution obtained from Gaussian noise matched to the phantom noise level.
Right: ILC distribution obtained from the phantom.

ject, the T_1-weighted anatomical images and the statistical parametric maps were spatially transformed to MNI space. The voxels common to the statistical parametric maps from all three runs were overlaid onto that subject's anatomical image for display.

Reproducibility

fMRI data obtained from repeated resting-state runs in the second experiment were used to test the reproducibility of the tissue-specific pattern in three healthy subjects. ILC maps were obtained for all three runs, and the correlation coefficient between them was ascertained to assess reproducibility [Strother et al., 1997].

Differentiating experimental conditions

ILC maps were generated for the resting state (Condition 1) and continuous motor (Condition 2) separately, and the difference between the maps of the two conditions was obtained to assess changes in local coherence. It has been reported that the default mode network is deactivated during the performance of an explicit task when compared with resting state [Raichle et al., 2001]. Based on this, the difference in maps may highlight this network.

Comparison of ILC and ReHo

We performed an explicit comparison of ILC with ReHo by evaluating their tissue specificity and within tissue variance. ILC and ReHo [Zang et al., 2004] maps were calculated from the data obtained in the second experiment. Histograms of ILC and ReHo maps were plotted and the statistical significance of the difference between their gray matter and white matter distributions was ascertained. The ability of ILC and ReHo to differentiate between the tissues demonstrates their sensitivities to fMRI physiology and neural processing in the tissues [Deshpande et al., 2006; Kruger and Glover, 2001].

Statistical Significance Testing

We subjected the gray matter and white matter ILC distributions to a Jarque–Bera test for goodness-of-fit to a normal distribution [Jarque and Bera, 1980] and found that the distributions were not normal (at 95% significance). Hence, we employed the nonparametric Wilcoxon rank sum test [Wilcoxon, 1945] to test for the significance of the difference in tissue specific ILC distributions. This test was employed before and after physiological correction, and for high- and low-resolution data. For testing the

TABLE I. Mean ILC values of gray matter and white matter for high and low-resolution data

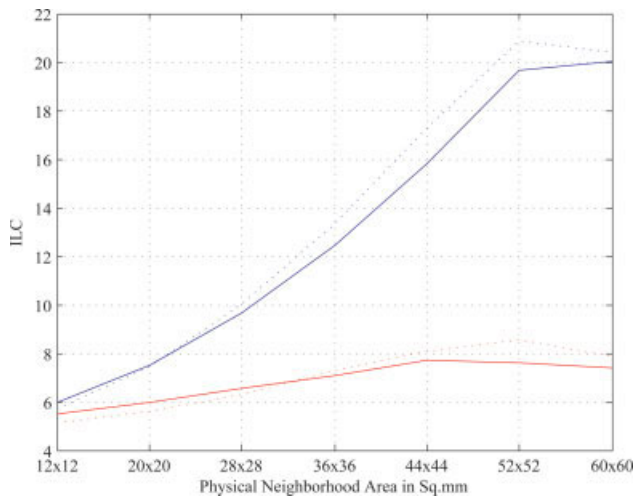| Subject	Gray matter			White matter		
	High resolution	Low resolution	*P*-value	High resolution	Low resolution	*P*-value
1	21.8	21.6	0.7	6.1	6.0	0.7
2	20.5	20.3	0.4	7.9	7.6	0.3
3	23.6	23.2	0.8	7.4	7.2	0.6

Figure 6.

Variation of ILC with increasing neighborhood size for both high (dotted line) and low-resolution data (solid line). Blue: gray matter. Red: white matter.

significance of the difference between ILC values of each voxel and the gray matter mean ILC, the gray matter distribution was ascertained. Subsequently, the position of the

TABLE II. Effect of physiological rhythms on ILC

	Gray matter			White matter		
Subject	BC	AC	P-value	BC	AC	P-value
4	21.7	22.7	0.35	11.4	12.0	0.34
5	27.9	28.1	0.76	11.8	11.7	0.89
6	26.3	26.7	0.59	8.1	8.3	0.66

BC, before correction for physiological noise; AC, after correction.

ILC value of every voxel in the corresponding gray matter distribution was calculated. To estimate the P-value of each voxel's ILC, the fraction of gray matter voxels with ILC above it was ascertained. This procedure was adopted instead of the t-test since the gray matter distributions were not normal.

RESULTS AND DISCUSSION

Inherent Correlation in fMRI Data and its Correction

The average spatial correlation functions for the phantom and the brain tissue, respectively, are shown in Figure 1.
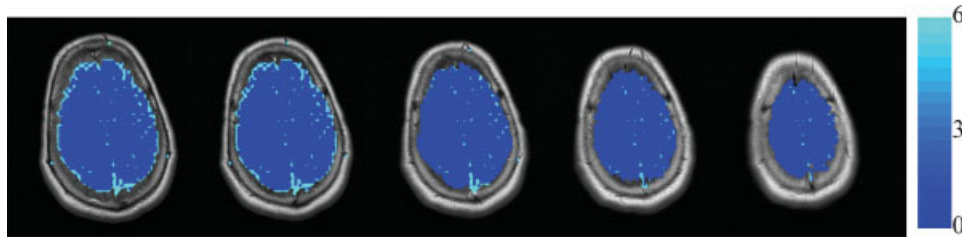

Figure 7.

ILC difference maps obtained by subtracting the ILC maps before and after correcting for physiological noise.
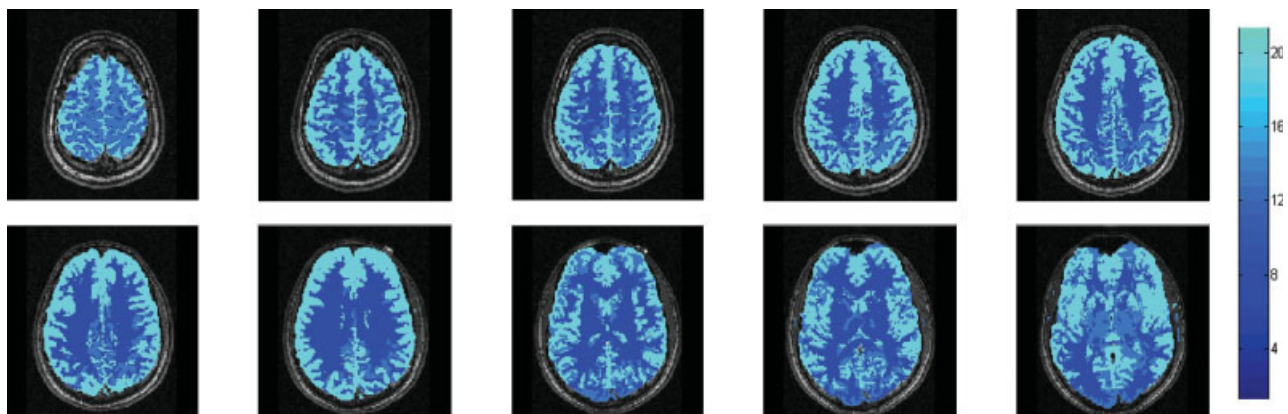

Figure 8.

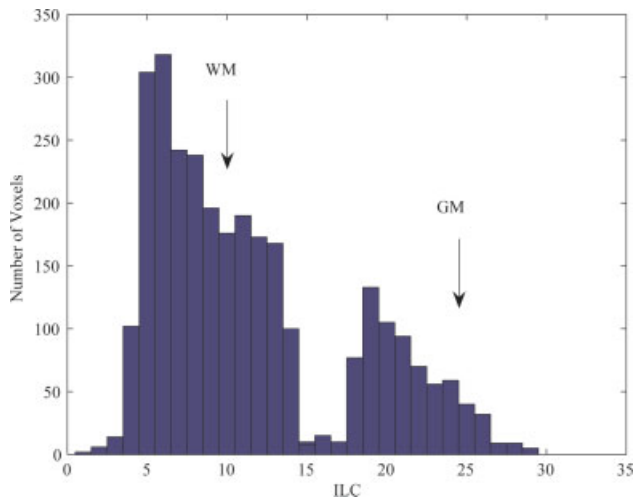ILC maps during resting-state indicating the tissue specificity of ILC.

Figure 9.

Histogram of ILC values showing separable gray matter and white matter distributions.

TABLE III. Correlation coefficient between ILC maps obtained from repeated runs demonstrating reproducibility

Subject	Run 1 and Run 2	Run 1 and Run 3	Run 2 and Run 3
1	0.94	0.94	0.95
2	0.93	0.91	0.94
3	0.84	0.83	0.91

A rescaled version of the phantom's spatial correlation function is depicted in Figure 3, which shows a *sinc* modulation in the readout direction. This is likely the result of inherent filtering caused by the interpolation of data sampled on the readout gradient ramps in the EPI sequence. In EPI, a finite time is needed to switch the readout gradient from the positive value to the negative value. Sometimes, as is the case here, data are sampled on the ramps and interpolation has to be performed in the k-space during image reconstruction, leading to the *sinc* modulation in Figure 3. The ILC map for the phantom is
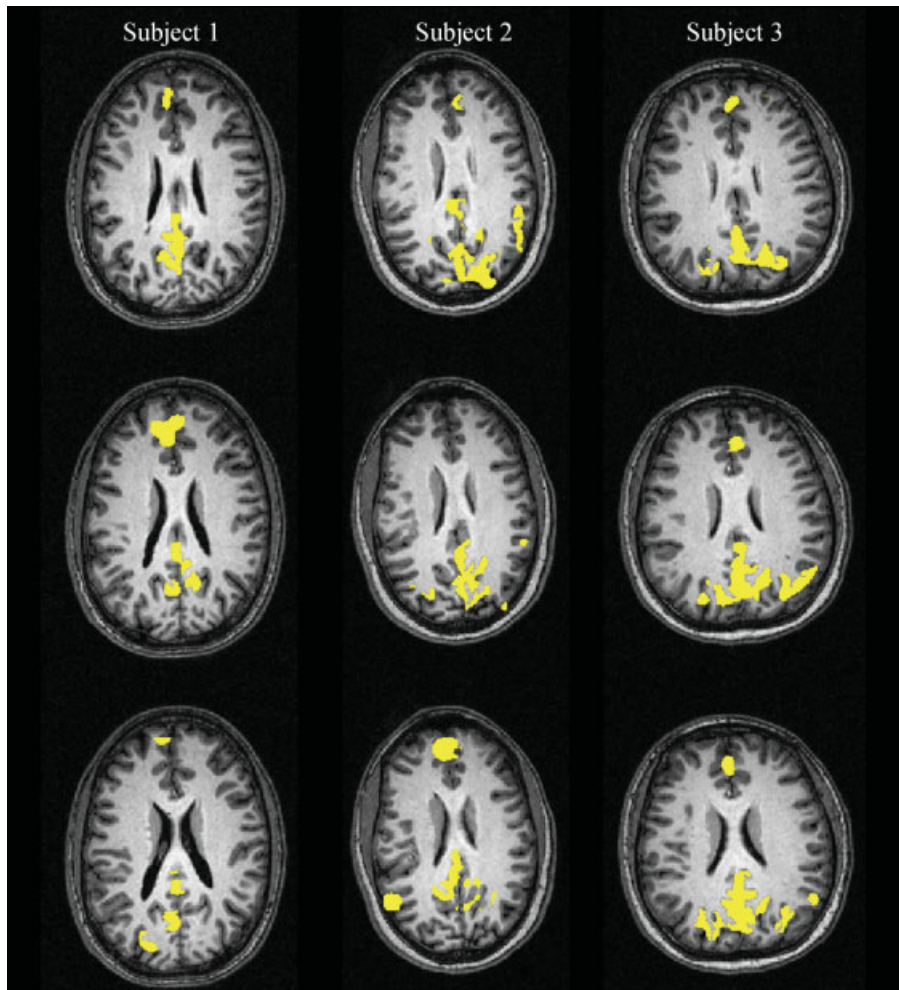

Figure 10.

Regions having ILC values significantly different from the mean gray matter ILC for the three subjects. The three slices shown in each subject are those containing the majority of voxels exhibiting significantly higher ILC.
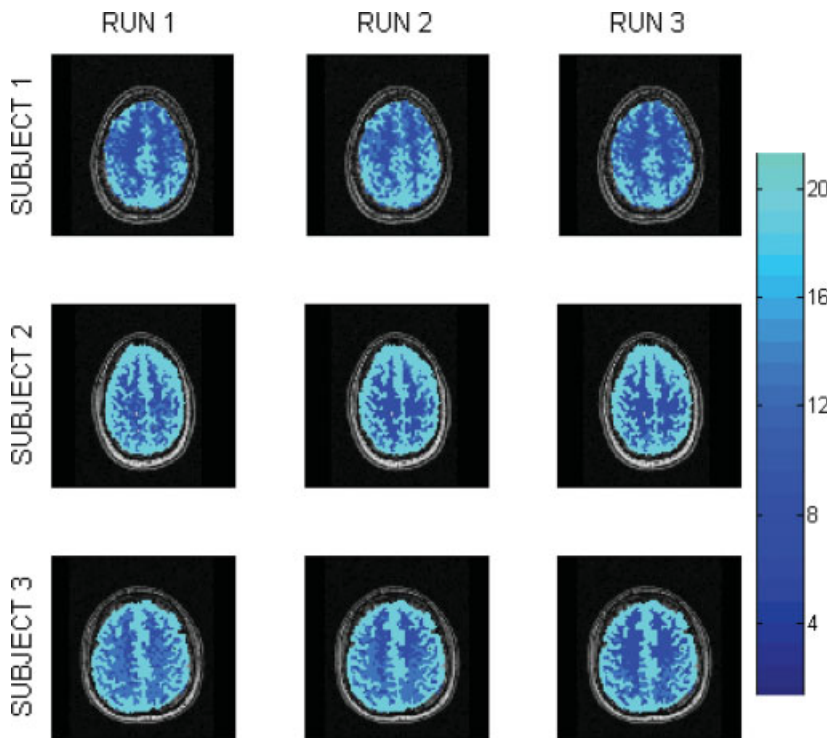
Figure 11.
ILC maps for three consecutive resting-state runs in healthy individuals. The images are representative of a typical slice and other slices also gave similar results.
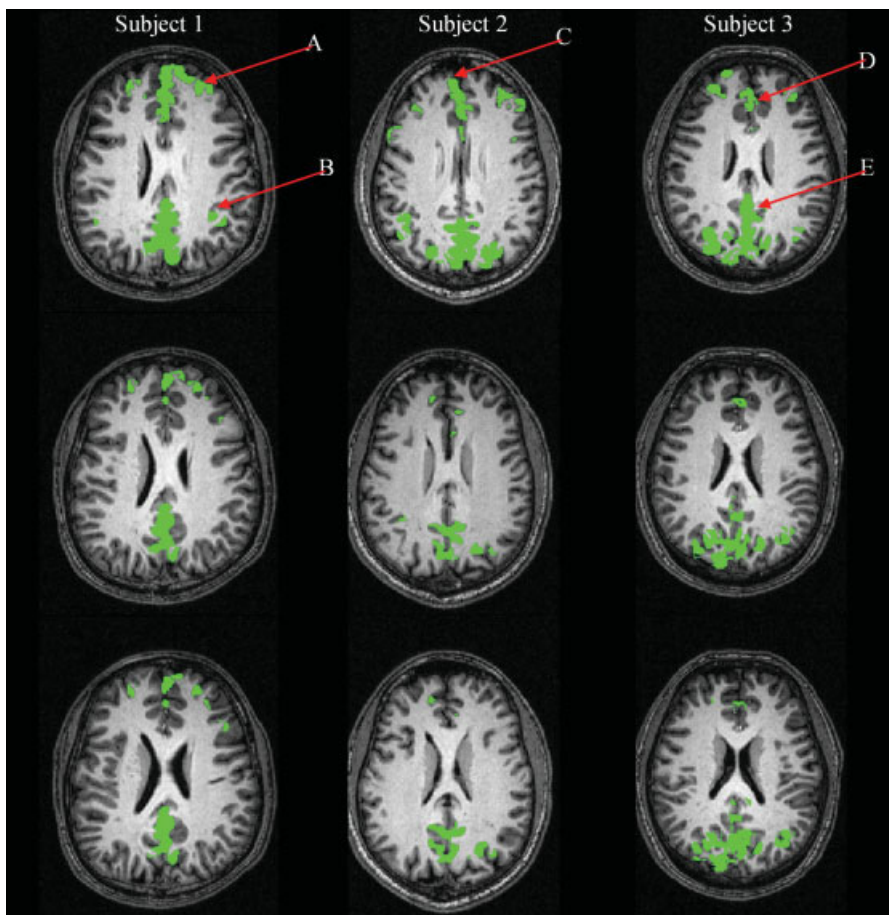

Figure 12.
ILC difference maps showing the regions having higher ILC during resting state when compared with the continuous motor condition. Note that the maps were thresholded at a *P*-value of 0.05. The regions indicated are (**A**) lateral prefrontal cortex (LPFC), (**B**) inferior parietal cortex (IPC), (**C**) medial prefrontal cortex (MPFC), (**D**) dorsal anterior cingulate cortex (dACC), and (**E**) posterior cingulate cortex (PCC) extending rostrally into precuneus. The slices containing the components of the default mode network are displayed for each subject.

shown in Figure 4. Although the mean value of phantom ILC is substantially less than that of brain tissue, the distribution of phantom ILC is significantly different from the null distribution (Fig. 5), indicating non-negligible inherent correlation. Therefore, we subtracted the average spatial correlation function of the phantom from the spatial correlation function of the brain tissue pixels before calculating ILC.

It is worth noting that global variations in signal time courses may lead to global correlations that result in elevated ILC values. This could be addressed by removing the global mean [Fox et al., 2005, 2006; Fransson, 2005; Greicius et al., 2003]. In our data, this was not found to be a significant factor and global mean correction did not alter the difference between ILC values of gray matter and white matter.

Discretization

As we explained in the Introduction section, a major advantage of the ILC method is its independence of the image resolution. Table I lists the mean gray matter and white matter ILC values calculated for using high- and low-resolution images. The Wilcoxon rank sum test shows that there is no significant difference between the two resolutions.

Truncation

Figure 6 plots the ILCs, calculated with low- and high-resolution images, respectively, versus the neighborhood size used. It can be seen that the ILC plateaus at 52×52 mm^2, indicating that correlation beyond this distance is negligible, were in agreement with a recent work [Bellec et al., 2006]. This result also indicates that for the calculation of ILC, as long as a sufficiently large neighborhood is used, the result is independent of the neighborhood size. In this work, we employed a 60×60-mm^2 neighborhood. Also, the high- and low-resolution curves follow each other closely, reinforcing the fact that ILC is independent of image resolution.

Effect of Physiological Noise

As shown in both Table II and Figure 7, the removal of respiratory and cardiac noise did not significantly alter the ILC values in gray matter and white matter. In fact, the Wilcoxon rank sum test showed that the difference in the tissue ILCs before and after correction is not significant. The difference map in Figure 7 shows that most voxels were not affected by the correction, with few voxels in isolated areas in the proximity of large vessels and cerebrospinal fluid exhibiting detectable differences.

In contrast to ReHo [Zang et al., 2004], our approach does not require the specification of a particular neighborhood size, is independent of image resolution, and does not need spatial smoothing. In addition, we showed that
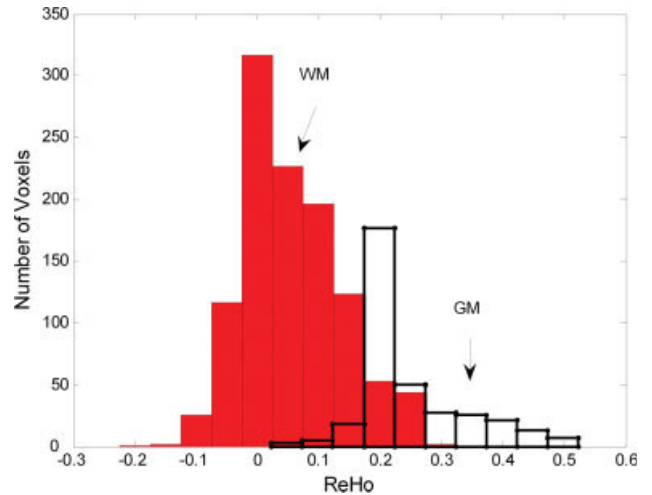

Figure 13.

Histograms of the ReHo values of the white matter (WM) and gray matter (GM). This histogram is derived from the data of the subject shown in Figure 9. Based on these histograms it is difficult to separate the gray matter from the white matter based on ReHo values.

the inherent correlation in our images could not be ignored and hence we compensated for its effects; while we examined this inherent correlation only on our scanner, data acquired with other scanners are likely to contain similar inherent correlation that should be accounted for. Also, as we have shown, physiological fluctuations have little contribution to gray matter and white matter ILC values. These features make ILC a more robust measure for characterizing local coherence.

Tissue-specificity

ILC was found to be tissue-specific as shown in Figure 8 for a representative subject. The corresponding mean ILC values for gray matter and white matter are shown in Tables I–II. The P-values of the Wilcoxon rank sum test are less than 10^{-20} for all the subjects, indicating that white matter and gray matter ILC distributions are significantly different. ILC is higher in the gray matter than that in the white matter (a fact also apparent in the gray matter and white matter distributions shown in Fig. 9). This difference possibly reflects a combination of neuronal and hemodynamic factors that have been implicated in earlier reports of differences between gray matter and white matter [Deshpande et al., 2006; Kruger and Glover, 2001].

Regional ILC Differences in Gray Matter

Figure 10 shows the regions having ILC values significantly higher than the mean gray matter ILC for the three subjects from the second experiment. It is evident that the components of the default mode network, particularly

TABLE IV. Mean ILC and KCC values of gray matter and white matter

Subject	ILC			KCC		
	Gray matter	White matter	*P*-value	Gray matter	White matter	*P*-value
1	21.6	6.0	0	0.20	0.04	0.10
2	20.3	7.6	0	0.18	0.05	0.12
3	23.2	7.2	0	0.26	0.05	0.05

posterior and anterior cingulate cortices, have significantly higher ILC compared with other gray matter regions. This result is consistent with previous studies that have reported significantly higher regional cerebral blood flow [Raichle et al., 2001] and ReHo values [He et al., 2004] in the default mode network.

Reproducibility

Table III lists the correlation coefficients between the ILC maps obtained from three repeated runs in three subjects. It is clear that there is a high degree of consistency between them. The resting-state ILC maps for all the three subjects are shown in Figure 11. In these maps tissue-specific patterns are consistent across consecutive resting-state runs. Note that the value and the spatial patterns of the phantom ILC (Fig. 4) are significantly different from those shown in Figure 11, confirming that the tissue-specific resting-state pattern is not due to the inherent correlation.

Differentiating Experimental Conditions

It is evident from the ILC difference maps shown in Figure 12 that there is a reduction of local coherence in the default mode network during the continuous motor task when compared with resting state. This is consistent with previous reports of deactivation of the default mode network during the performance of an explicit task when compared with resting state [Raichle et al., 2001]. This result shows that ILC could be an useful measure to capture ROI-specific changes in local coherence with different experimental conditions. Interestingly, the continuous motor task did not alter the ILC values in the motor network significantly similar to a lack of change in inter-regional connectivity in the network reported in a previous study [Morgan and Price, 2004].

Comparison of ILC and ReHo

As shown in Table IV, the difference between gray and white matter distributions was only significant in one subject for ReHo while it was significant in all three subjects for ILC. A comparison of gray matter and white matter ReHo distributions shown in Figure 13 with that of the corresponding ILC distributions in Figure 9 confirms the results shown in Table IV. Previous studies [Deshpande et al., 2006; Kruger and Glover, 2001] have attributed tissue specificity

in the brain to differences in fMRI physiology and neural processing. Our results show that ILC may be more sensitive to these differences when compared with ReHo.

We have provided a comparison between ILC and ReHo since ReHo also attempts to characterize local coherence in a voxel neighborhood. It should also be noted that another technique, Cross-correlation Coefficients of Spontaneous Low Frequency (COSLOF) [Li et al., 2002], which was originally introduced to measure average inter-regional correlation, could be made equivalent to ILC if the COSLOF calculation is done with correlations between a given voxel and its neighborhood.

CONCLUSIONS

In this article, we have introduced and characterized a general measure, ILC, to quantify local brain coherence. We hypothesized and demonstrated that ILC is effectively independent of image resolution and the neighborhood size as long as it is sufficiently large. In addition, we also found that respiratory and cardiac fluctuations do not significantly affect ILC values in brain tissue. Furthermore, the inherent correlation in the data was found to be small but non-negligible, and a correction was introduced. As a demonstration of biological relevance, reproducible, tissue-specific ILC patterns were found in the resting-state fMRI data of healthy individuals and discriminated between gray and white matters. Within the gray matter, the default mode network exhibited higher ILC in resting state. The reduction of ILC in the default mode network during a continuous motor task when compared with the resting state showed the utility of ILC in discriminating experimental conditions. Also ILC was shown to discriminate between different tissues better than ReHo. It is concluded that the ILC measure is a robust tool to assess local brain coherence.

REFERENCES

Baumgartner R, Somorjai R, Summers R, Richter W (1999): Assessment of cluster homogeneity in fMRI data using Kendall's coefficient of concordance. Magn Reson Imaging 17:1525–1532.

Bellec P, Perlbarg V, Jbabdi S, Pelegrini-Issac M, Anton J, Doyon J, Benali H (2006): Identification of large-scale networks in the brain using fMRI. Neuroimage 29:1231–1243.

Biswal B, Yetkin FZ, Haughton VM, Hyde JS (1995): Functional connectivity in the motor cortex of resting human brain using echo-planar MRI. Magn Reson Med 34:537–541.

Biswal B, VanKylen J, Hyde JS (1997): Simultaneous assessment of flow and BOLD signals in resting-state functional connectivity maps. NMR Biomed 10:165–170.

Cordes D, Haughton VM, Arfanakis K, Wendt GJ, Turski PA, Moritz CH, Quigley MA, Meyerand ME (2000): Mapping functionally related regions of brain with functional connectivity MR imaging. Am J Neuroradiol 21:1636–1644.

Deshpande G, LaConte S, Peltier S, Hu X (2006): Tissue specificity of nonlinear dynamics in baseline fMRI. Magn Reson Med 55:626–632.

Fox MD, Snyder AZ, Vincent JL, Corbetta M, Van Essen DC, Raichle ME (2005): The human brain is intrinsically organized into dynamic, anticorrelated functional networks. Proc Natl Acad Sci USA 102:9673–9678.

Fox MD, Corbetta M, Snyder AZ, Vincent JL, Raichle ME (2006): Spontaneous neuronal activity distinguishes human dorsal and ventral attention systems. Proc Natl Acad Sci USA 103:10046–10051.

Fransson P (2005): Spontaneous low-frequency BOLD signal fluctuations: An fMRI investigation of the resting-state default mode of brain function hypothesis. Hum Brain Mapp 26:15–29.

Friston KJ, Frith CD, Liddle PF, Frackowiak RSJ (1993): Functional connectivity—The principal-component analysis of large (PET) data sets. J Cereb Blood Flow Metab 13:5–14.

Greicius MD, Krasnow B, Reiss AL, Menon V (2003): Functional connectivity in the resting brain: A network analysis of the default mode hypothesis. Proc Natl Acad Sci USA 100:253–258.

Hampson M, Peterson BS, Skudlarski P, Gatenby JC, Gore JC (2002): Detection of functional connectivity using temporal correlations in MR images. Hum Brain Mapp 15:247–262.

He Y, Zang YF, Jiang TZ, Liang M, Gong GL (2004): Detecting functional connectivity of the cerebellum using low frequency fluctuations (LFFs). Lect Notes Comput Sci 3217:907–915.

Hu X, Le TH, Parrish T, Erhard P (1995): Retrospective estimation and correction of physiological fluctuation in functional MRI. Magn Reson Med 34:201–212.

Jarque CM, Bera AK (1980): Efficient tests for normality, homoscedasticity and serial independence of regression residuals. Econ Lett 6:255–259.

Kendall M, Gibbons J (1990): Rank Correlation Methods. Oxford University Press: New York (5th edition).

Kriegeskorte N, Goebel R, Bandettini P (2006): Information-based functional brain mapping. PNAS 103:3863–3868.

Kruger G, Glover GH (2001): Physiological noise in oxygenation-sensitive magnetic resonance imaging. Magn Reson Med 46:631–637.

Li SJ, Li Z, Wu G, Zhang MJ, Franczak M, Antuono PG (2002): Alzheimer disease: Evaluation of a function MR imaging index as a marker. Radiology 225:253–259.

Lowe MJ, Mock BJ, Sorenson JA (1998): Functional connectivity in single and multislice echoplanar imaging using resting-state fluctuations. Neuroimage 7:119–132.

Morgan VL, Price RR (2004): The effect of sensorimotor activation on functional connectivity mapping with MRI. Magn Reson Imag 22:1069–1075.

Mugler J, Brookeman J (1990): Three-dimensional magnetization-prepared rapid gradient-echo imaging (3D MP RAGE). Magn Reson Med 15:152–157.

Peltier SJ, Noll DC (2000): T_2* dependence of functional connectivity. Neuroimage 16:985–992.

Raichle ME, MacLeod AM, Snyder AZ, Powers WJ, Gusnard DA, Shulman GL (2001): A default mode of brain function. Proc Natl Acad Sci USA 98:676–682.

Rorden C, Brett M (2000): Stereotaxic display of brain lesions. Behav Neurol 12:191–200.

Strother SC, Lange N, Anderson JR, Schaper KA, Rehm K, Hansen LK, Rottenberg DA (1997): Activation pattern reproducibility: Measuring the effects of group size and data analysis models. Hum Brain Mapp 5:312–316.

Wilcoxon F (1945): Individual comparisons by ranking methods. Biometrics 1:80–83.

Zang Y, Jiang T, Lu Y, He Y, Tian L (2004): Regional homogeneity approach to fMRI data analysis. Neuroimage 22:394–400.